ENGINEERING CHARGE TRANSFER AND STABILITY IN A CONFINED SYSTEM: ATOMIC TI^{4+} SITES WITHIN A MESOPOROUS SILICA MATRIX

Nasrine-Dalila TOUAA [1], Mohammed Mustapha BOUHENT [2], Kahina BENTALEB[1], Abdelkader BENDERRAG[1], Leila SAKER [3], Rachida OUARGLI SAKER[3], Zohra BOUBERKA[1], Narjess BELHADJ [4], Ulrich MASCHKE [5,*]

A model system has been developed to study the effect of spatial confinement on the stability of photocatalysis. This system consists of Ti^{4+} sites dispersed throughout an SBA-15 silica framework. Tetrahedral Ti centres (0.47 wt%) were detected with a charge-transfer band at 220 nm. The photo-oxidation kinetics of a molecular probe were examined and found to follow a pseudo-first-order model influenced by interfacial electrostatics. Less than 10% activity loss was observed over four photocatalytic cycles, demonstrating the system's exceptional durability. This surpasses the performance of nanoparticle composites because deactivation pathways caused by framework confinement are minimized. A general physical principle has been established to explain the stability of catalytic processes at interfaces.

Keywords: Mesoporous materials; Catalyst stability; Confinement effects; Charge transfer; Kinetic modeling; Physical model; Structure-property relationships.

1. Introduction

For several years, the activities of our research group have focused on developing stable, functional materials for a range of applications, from adsorption to photocatalysis. One of our main objectives is to improve material

* Corresponding author
[1] Laboratoire de Physico-Chimie des Matériaux, Catalyse et Environnement (LPCM-CE), Université des Sciences et de la Technologie d'Oran Mohamed Boudiaf (USTOMB), Faculté de Chimie, BP 1505, El M'naouer, 31000 Oran, Algeria
[2] Laboratoire de l'Ingénierie des Procédés de l'Environnement (LIPE), Université des Sciences et de la Technologie d'Oran Mohamed Boudiaf (USTOMB), BP 1505, El M'naouer, 31000 Oran, Algeria
[3] Laboratoire Sciences, Technologie et Génie des Procédés (LSTGP), Faculté de Chimie, Université des Sciences et de la Technologie d'Oran Mohamed Boudiaf (USTOMB), BP 1505, El M'naouer, 31000 Oran, Algeria
[4] Laboratoire chimie des polymères (LCP), Faculté des sciences exactes et appliquées, Université Oran1 Ahmed Ben Bella, B.P 1505, El M'naouer, 31000 Oran, Algeria
[5] Unité Matériaux et Transformations (UMET), UMR 8207, Université de Lille, CNRS, INRAE, Centrale Lille, 59000 Lille, France

efficiency while ensuring that the materials can be recycled several times after use. To this end, we have explored an approach involving the incorporation of isolated, discrete active centres within a robust, inert host matrix. This approach provides a controlled platform for investigating and tuning critical physical phenomena. These include interfacial charge transfer and the stability of catalytic cycles. At the same time, it enables us to better understand fundamental structure–property relationships related to quantum and statistical mechanics [1, 2].

Heterogeneous photocatalysis offers an attractive experimental framework for implementing this strategy. The efficiency of photocatalytic processes, such as the light-driven degradation of organic pollutants, depends on complex interactions. The most important factors are how the material absorbs light, how it generates and uses electricity, and how long it can perform effectively in real-world conditions [3, 4]. Titanium dioxide (TiO_2), the standard material in this field, has two key issues: active sites on the surface degrade over time and photogenerated electrons and holes recombine quickly, which limits its performance [5, 6].

These limitations can be overcome by confining the active species within a custom-made host material, which is a widely adopted approach. The large surface areas of mesoporous silicas make them ideal for this purpose. Their chemical adaptability and well-defined pore networks are also beneficial, as demonstrated by SBA-15, for instance [7, 8]. Some authors [9,10] dispersed the pre-formed TiO_2 nanoparticles (NPs) on certain silica surfaces. Although this has proven to be a method to obtain composites combining the photocatalytic activity of TiO_2 with the enhanced adsorption capacity of the porous host material, these systems degrade rapidly, either due to metal dissolution or NPs agglomeration. The long-term reliability of these substances is being affected by important errors.

To increase the lifetime of the composite, we study whether arranging the atoms in a rigid structure has a beneficial effect. This approach considers the addition of Titanium during the formation of the SBA-15 silica network. This avoids the formation of Titanium NPs that could aggregate or separate.

In this article, the probe used is Orange G dye and it is analyzed how certain parameters such as pH and concentration influence the process, applying models that consider the influence of charges and surface electrical interactions [11,12]. The results presented here can be used in future studies related to catalyst deactivation.

2. Experimental Framework: System Fabrication and Property Measurement

2.1. Materials and Model System

All the chemicals used in this study were of analytical grade. They were used without further purification. Pluronic® P123 ($EO_{20}PO_{70}EO_{20}$) was utilized as the structure-directing agent, exhibiting an average molecular weight of

approximately 5,800 g/mol. Tetraethyl orthosilicate (TEOS, ≥98% purity) and Titanium(IV) chloride ($TiCl_4$, 97% purity) were employed as the silica and Titanium precursors, respectively. In order to establish and sustain an acidic environment, hydrochloric acid (HCl, 37%) was utilized. Orange G (OG, $C_{16}H_{10}N_2Na_2O_7S_2$) is a diazo dye with a distinct absorption maximum at 478 nm that has stable anionic sulfonate groups. OG was used as the molecular probe to investigate interfacial electrostatic interactions in photocatalytic degradation studies. The pH level of the reaction solutions was modulated through the application of sodium hydroxide (NaOH).

2.2. Synthesis of the Confined Active-Site Model (Ti-SBA-15)

To stop the development of oxide zones by titanium particles by trapping them in the silica structure, the "direct co-condensation" method was used, as in [9]. The original part consisted of the direct placement of Ti^{4+} into the forming Si-O-Si network. The process consisted of the following steps: a) dissolving Pluronic P123 (3.0 g) in deionized water (140 mL) at 35 °C. b) adding concentrated HCl (12 mL, 37%); c) Under vigorous stirring, 6.8 mL of TEOS was slowly added. d) hydrolysis, resulting in the formation of oligomers over 1 hour. e) Adding a pre-measured amount of $TiCl_4$, pre-diluted in chilled ethanol, in order to obtain a Si/Ti molar ratio of 50. The acidic environment in which the work was carried out acted as a kinetic barrier. Thus, the Ti-O-Ti condensation rate was reduced in favor of isolated Ti-O-Si bonds.

The mixture was subsequently subjected to an aging process at 35°C for a duration of 24 h, thereby enabling the micelles to undergo organization. It was then subjected to hydrothermal treatment at 100 °C for a further 24 h to solidify the inorganic network. The solid was collected using a filter, washed with clean water, and dried. Subsequently, the samples were exposed to air at 550°C for 5 h at a rate of 1°C/min. This process was undertaken to ensure the complete removal of the templates without compromising the integrity of the samples. We used the same process to prepare a Titanium-free SBA-15 control material, except we omitted $TiCl_4$.

2.3. Structural and Electronic Characterization

We used a few different methods to study the structure and chemicals in the materials. The long-range hexagonal mesoporosity characteristic of SBA-15 was confirmed by low-angle patterns obtained by X-ray diffraction (XRD). The lack of noticeable diffraction features in the wide-angle region ruled out the presence of crystalline Titania phases. This supports the idea that Titanium is atomically dispersed. The electronic signature of Titanium was revealed through UV-Vis diffuse reflectance spectroscopy (DRS).

The available data were used to estimate the optical band gap, using the Tauc plot analysis. Fourier-transform infrared spectroscopy (FTIR) furnished

further evidence in the form of vibrational spectra and confirmed the incorporation of Ti into the framework.

Scanning electron microscopy (SEM) combined with energy-dispersive X-ray spectroscopy (EDS) offered insights into the morphology and the quantitative composition of the samples. The structure is indicative of the material, as evidenced by the microscopic images. Additionally, a titanium loading of 0.47 wt% was revealed by spectroscopic analysis. We chose this concentration to keep the site isolated. Thermogravimetric analysis (TGA) was employed to evaluate the thermal degradation behavior of the materials, the removal of the organic template during calcination and the stability of the inorganic resulted structure.

2.4. Photocatalytic Activity and Stability Assessment

To determine the photocatalytic activity, the The degradation of OG in an aqueous suspension under UV irradiation (LC3 source-Hamamatsu, wavelength 365 nm) was studied. Previously, the suspension was stirred in d the dark for 60 min. A thermostatted reactor at 25±1°C with continuous agitation was used.

After UV illumination, the decrease in OG concentration was measured using its specific absorbance at 478 nm. The reaction rates were studied with a pseudo-first-order model [11], being in agreement with it. Equation (1) allows the determination of the gradient k, denoting the apparent rate constant:

$$\mathrm{Ln}\,(C_0 / C_t) = k\,t \tag{1}$$

where $C_t \equiv C(t)$ denotes the concentration at time t, and $C_0 \equiv C\,(t{=}0)$ is the initial concentration after the dark adsorption period mentioned.

The model was validated by linear regression of the converted data ($R^2 > 0.98$ in all cases). The factors influencing the reaction rate were obtained after methodically varying the following parameters: the pH of the solution was adjusted within the range of 2–10. The initial OG concentration was between 10 and 50 mg/L. The range of catalyst loading used was from 0.5 to 3.0 g L^{-1}. For reliability, each condition was tested twice or three times.

In order to obtain the stability of the catalyst, four consecutive cycles were performed. After each cycle, we recovered the solid by filtration and washed it with water and ethanol. It was then dried at 80 °C and reused under the same conditions.

2.5. Control Experiments for Mechanism Elucidation

To make sure the degradation really came from photocatalysis, we ran three control experiments: photolysis (light alone, no catalyst), adsorption (catalyst in the dark), and a matrix control with pure silica. Ti-SBA-15 was significantly more active than all three, confirming that the degradation was due to photoactivated processes at the isolated Titanium sites.

3. Results and Discussion

3.1. Structural Validation of the Confined Active-Site Model

The structural integrity and atomic dispersion of Titanium within the Ti-SBA-15 framework were investigated using XRD.

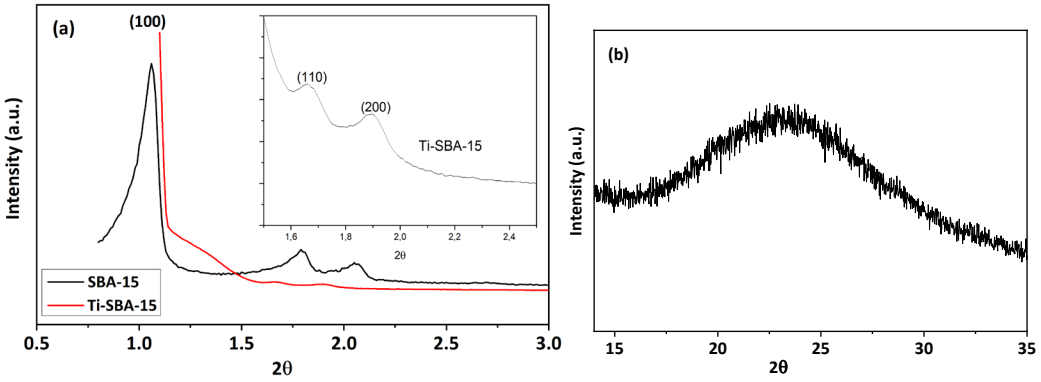

Fig. 1. X-ray diffraction patterns of Ti-SBA-15: (a) low-angle region confirming the 2D-hexagonal mesostructure; (b) wide-angle region demonstrating the absence of crystalline TiO_2 phases.

The low-angle XRD pattern (Fig. 1a) exhibits the (100), (110) and (200) reflections that are characteristic of a well-ordered, two-dimensional, hexagonal lattice (space group P6mm). This confirms that the synthesis successfully replicated the highly ordered, mesoporous architecture of SBA-15 [13]. The primary (100) reflection, which is observed at a d-spacing of 65.9 Å, corresponds to a unit cell parameter of a_0 = 76.1 Å. This represents a measurable lattice expansion compared to pure silica SBA-15.

The presented data show the isomorphic substitution of the Si^{4+} ion (ionic radius ~0.40 Å) with the larger Ti^{4+} ion (~0.60 Å) inside the walls of the structural framework [14, 15]. The shape and arrangement of these peaks lead to the conclusion that the long-range mesoscopic order of the silica host is maintained. The porosity of the material was not affected by the Ti inclusion.

As shown in Fig. 1b, there appears to be an absence of discernible Bragg peaks in the wide-angle XRD pattern. This is especially true of those associated with crystalline TiO_2 phases such as anatase or rutile. The absence of Titanium is significant. This confirms that it is incorporated within the amorphous silica framework. It is a constituent of the Titanium atom (Ti^{4+}). This is in contrast to its presence in the form of TiO_2 nanoparticles [16]. This means there is strong proof that the Si^{4+} ion (with a radius of ~0.40 Å) can be replaced by the larger Ti^{4+} ion (~0.60 Å) in the framework walls. The sharpness and resolution of these peaks stay the same, which indicates that the mesoscopic long-range order of the silica host is preserved. The porosity of the material will not be compromised by the

inclusion of Ti. As will be discussed later, the material's performance is made possible by this unique configuration. Importantly, it is expected to prevent charge recombination while allowing reactants to diffuse through the open pore network without any obstacles [17, 18].

The morphology of the material obtained using SEM is shown in Fig. 2. This reveals uniform particles. These particles are either spherical or short, rod-like. They typically range in size from 0.5 to 1.0 μm. The particles have smooth surfaces and a clearly visible, well-interconnected porous texture. Importantly, there are no extra surface crystals visible, which supports the XRD results and rules out the presence of segregated TiO_2 nanoparticles. This uniform, exposed form performs an essential practical function. This can stop undesirable light diffusion and establish constant and repeatable mass transfer pathways required [19].

In Table 1 is presented the bulk composition of the Ti-SBA-15 sample obtained by Energy-dispersive X-ray spectroscopy (EDX) analysis. It is observed that Titanium is present in a small amount, 0.47% wt% (0.18 at%), proving the success of the isomorphic substitution. As expected, Titanium occupies isolated sites in the structure and does not form a distinct phase [20, 21].

Silicon (31.44 wt%) and oxygen (63.28 wt%) are the main elements in the silica matrix. Carbon (4.8 wt%) is an organic residue, having no effect on the desired properties of the material.

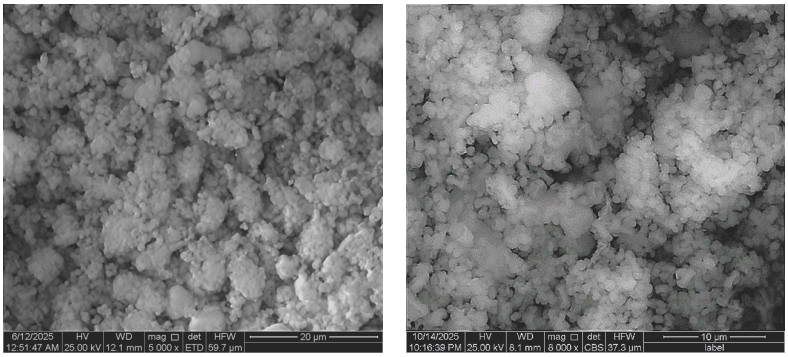

Fig. 2. SEM images of Ti-SBA-15..

Table 1.

Elemental composition of Ti-SBA-15 determined by EDX analysis

Element	Mass (%)	Atomic (%)
Si	31.44	20.40
O	63.28	72.10
Ti	0.47	0.18
C	4.82	7.32

The low overall Ti content (see Table 1) and the absence of crystalline TiO_2 signatures in wide-angle XRD (see Fig. 1b) show strong evidence of atomic dispersion, with almost no uncertainty. A single Ti–O–Si phase is present, containing uniformly dispersed Titanium cations. Because these are rigidly anchored in silica walls, the resulting material is stable [22, 23] and will therefore resist leaching and aggregation, while being available as a reactant. The resulting structure could be used when rapid charge movement is required, as in photocatalysis [24].

3.2. Electronic Structure Analysis via Optical Spectroscopy

The UV-Vis-DRS spectrum of the framework shown in Fig. 3 was used to study the the electronic state of Ti. The spectrum displays an important absorption maximum at 220 nm and unsignificant characteristics beyond 300 nm. The 220 nm band distinctly signifies the "ligand to metal charge transfer" (LMCT) transition ($O^{2-} \rightarrow Ti^{4+}$), which is anticipated for isolated Ti^{4+} in tetrahedral coordination [13, 14]. The total absence of the broad absorption edge is typically observed between 300 and 350 nm for TiO_2 NPs being a proof of atomic dispersion, in agreement with the structural evidence from XRD and EDX measurements [25].

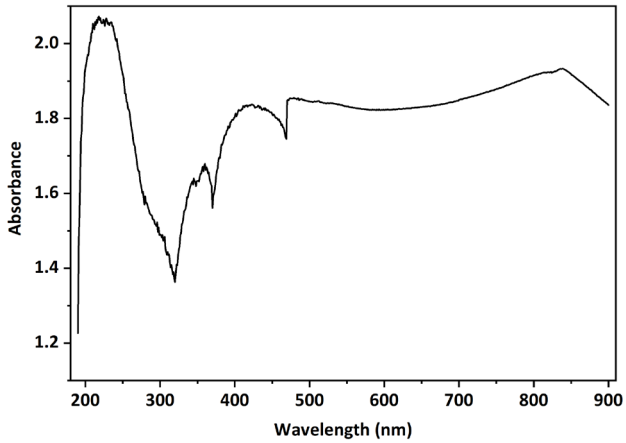

Fig. 3. UV-Vis-DRS of Ti-SBA-15 sample.

An optical band gap (E_g) of 3.8 eV for Ti-SBA-15 was revealed by the data analysis using a Tauc plot. This value is considerably higher than that of bulk anatase TiO_2 (~3.2 eV). It also surpasses the values reported for related materials, such as Ti-MCM-41, which typically range from 3.5 to 3.7 eV [26, 27]. We attribute this widened band gap to a pronounced quantum confinement effect, which occurs when the electrons are confined to a smaller space, resulting in a higher energy gap between the valence and conduction bands. The insulating silica matrix has a wide band gap, and within it, there are isolated individual Ti^{4+}

sites. They are also electronically decoupled, suppressing thus the formation of extended electronic states. This has two practical results. Firstly, it shifts the primary photoactivity to the UV range. Secondly, and more importantly, it suggests that photogenerated charge carriers (electrons and holes) have a higher intrinsic redox potential [27]. This could increase their driving force for oxidation reactions. Furthermore, a larger band gap can help reduce certain charge recombination mechanisms. This could potentially result in increased longevity for the carrier. This is beneficial for both catalytic efficiency and operational stability [28].

Using the Tauc plot, the activation enegy of Ti-SBA-15 was found to be E_g= 3.8 eV. This value is considerably higher than that of bulk anatase TiO_2 (~3.2 eV). It also surpasses the values reported for related materials, such as Ti-MCM-41, which usually range from 3.5 to 3.7 eV [26, 27]. We attribute this widened band gap to a quantum confinement effect, which occurs when the electrons are confined to a smaller space, resulting in a higher energy gap between the valence and conduction bands.

The insulating silica matrix has a wide band gap, and within it, there are isolated individual Ti^{4+} sites. They are also electronically decoupled, suppressing thus the formation of extended electronic states. This has two practical results: a) it shifts the primary photoactivity to the UV range, and b) it suggests that photogenerated electrons and holes have a higher intrinsic redox potential [27]. This could increase their driving force for oxidation reactions. Furthermore, a larger band gap can help reduce certain charge recombination mechanisms. This could potentially result in increased longevity for the charge carrier, thus improving the catalytic efficiency and operational stability [28].

3.3. Vibrational Spectroscopy: Probing Local Bonding Environments

A comparison of the FTIR spectra of SBA-15 and Ti-SBA-15 is shown in Fig. 4. The addition of Titanium does not alter the characteristic vibrations of the Si–O–Si framework, as demonstrated in [15]. A definitive spectral sign of successful incorporation is the emergence of a novel, separate band at ~960 cm^{-1} in the Ti-SBA-15 specimen. This band is clearly linked to the stretching vibration of Si–O–Ti linkages. Direct evidence of Titanium's covalent integration into the silica network is provided by this [28]. Furthermore, the lack of significant absorption in the 450–650 cm^{-1} range suggests the absence of Ti–O–Ti vibrations. These vibrations are characteristic of polymeric or nanocrystalline TiO_2 phases. This absence further supports our conclusion of atomic dispersion.

A comparison of the FTIR spectra of SBA-15 and Ti-SBA-15 is shown in Fig. 4. The addition of Titanium does not change the characteristic vibrations of the Si-O-Si structure, as demonstrated in [15]. A new band at ~960 cm^{-1} is also observed in the Ti-SBA-15 specimen, which is evidence of successful incorporation. This band is clearly related to the stretching vibration of the Si-O-

Ti bonds [28]. In addition, the lack of significant absorption in the range of 450-650 cm^{-1} suggests the absence of Ti-O-Ti vibrations. These vibrations are characteristic of polymeric or nanocrystalline phases of TiO_2. Their absence supports our conclusion regarding atomic dispersion.

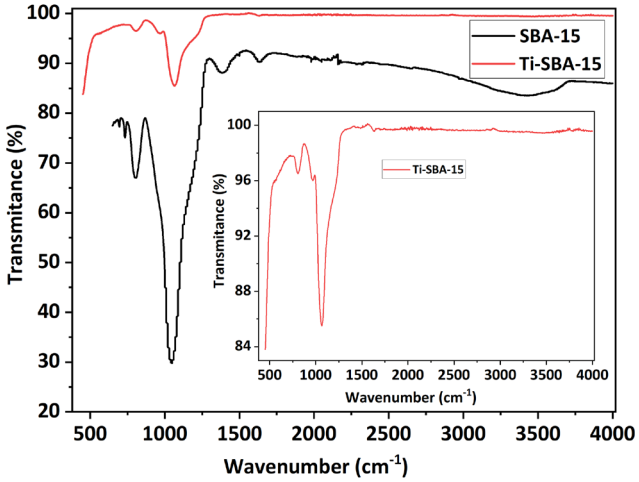

Fig. 4. FT-IR spectra of SBA-15 and Ti-SBA-15; Inset: the Si–O–Ti vibration band at ~960 cm^{-1}.

The slight rise in the strength of the wide O–H stretching band between 3000 and 3700 cm^{-1} indicates a greater number of surface silanol (Si–OH) and titanol (Ti–OH) groups. These hydroxyl groups are likely to play an important role in surface chemistry and the process of reactant adsorption during catalytic cycles [15].

3.4. Thermogravimetric Analysis: Assessing Framework Stability

Fig. 5 presents the TGA curves of as-synthesized SBA-15 and Ti-SBA-15. Both samples exhibit a multi-step mass loss profile. A pronounced weight loss below 100 °C is observed in the SBA-15 curve, which is attributed to the removal of physisorbed water or residual solvents from the synthesis. Above this temperature, the two curves follow a broadly comparable trend. The primary mass loss between 150 and 500 °C corresponds to the thermal decomposition of the organic template. For Ti-SBA-15, a small but consistent increase in mass loss is observed during this decomposition step, which may reflect altered interactions between the organic template and the Ti-modified framework.

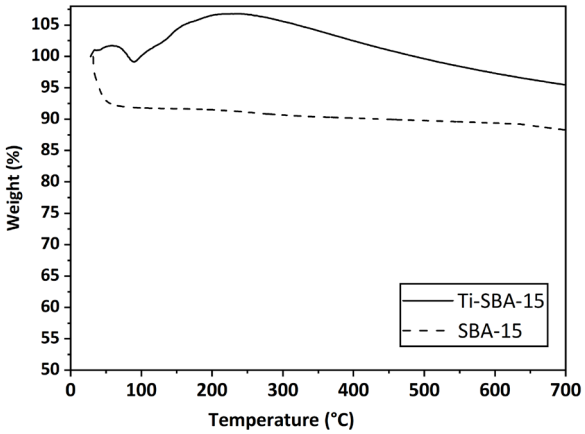

Fig. 5. TGA curves of as-synthesized SBA-15 and Ti-SBA-15.

Despite this deviation, both samples reach a stable mass plateau above 500 °C, confirming that the calcination protocol successfully yields a stable, purely inorganic framework. Thus, the incorporation of titanium preserves the overall thermal integrity of the SBA-15 architecture.

3.5. Functional Response: Kinetics, Parameter Dependence, and Stability Metrics

3.5.1. Mechanism Deconvolution and Kinetic Model

Fig. 6 shows the results of the control experiments that establish the limits of the system.

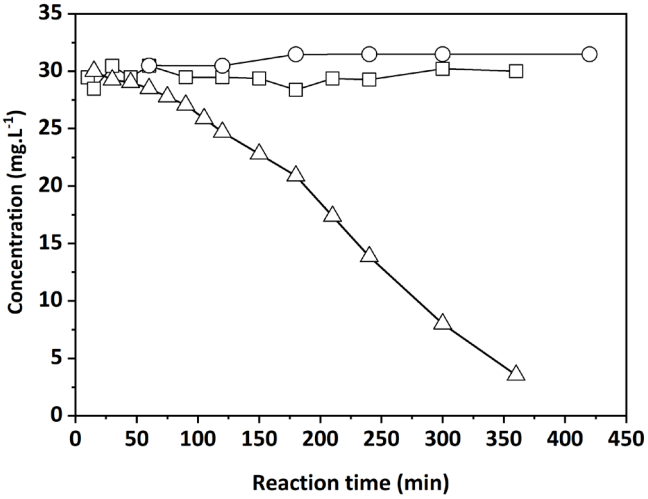

Fig. 6. Control experiments: photolysis (○), adsorption (□), and photocatalysis (Δ) with Ti-SBA-15.

The degradation of the OG probe only occurs when UV irradiation is present alongside Ti-SBA-15, confirming the photocatalytic mechanism on the Ti

framework sites. The time-dependent concentration decay (*C(t)*) is well described by a pseudo-first-order kinetic model. Thus, the apparent rate constant, *k*, [11] can be obtained.

3.5.2. Parameter Space Exploration and Mechanistic Insights

The practical reaction of the system was established by evaluating the apparent rate constant (*k*) in connection with essential operational variables. The rate constant increased with catalyst loading until it reached an optimum level.

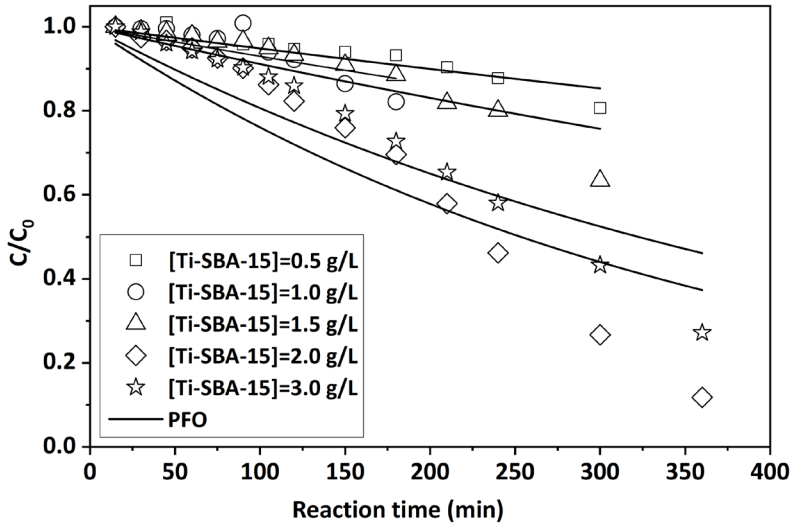

Fig. 7. Effect of Ti-SBA-15 loading on OG degradation.

The values were as follows : $k = 5.29 \times 10^{-4}$ min^{-1} at 0.5 g L^{-1}, $k = 7.29 \times 10^{-4}$ min^{-1} at 1.0 g L^{-1}, and $k = 9.27 \times 10^{-4}$ min^{-1} at 1.5 g L^{-1}. The maximum value of *k* was 2.74×10^{-3} min^{-1} at an optimal loading of 2.0 g L^{-1} (see Fig. 7). Beyond this point, *k* decreased to 2.15×10^{-3} min^{-1} at 3.0 g L^{-1} due to light scattering effects and reduced photon penetration. This phenomenon is well documented in slurry systems [21, 28, 29].

k also decreased monotonically with increasing initial OG concentration. It fell from 3.73×10^{-3} min^{-1} at 10 mg L^{-1} to 2.74×10^{-3} min^{-1} at 30 mg L^{-1}, and then to 9.82×10^{-4} min^{-1} at 50 mg L^{-1} (see Fig. 8). This trend indicates the onset of mass transport limitations and inner-filter effects. The probe molecule itself screens incident light. This reduces photon absorption by the catalyst [21, 28].

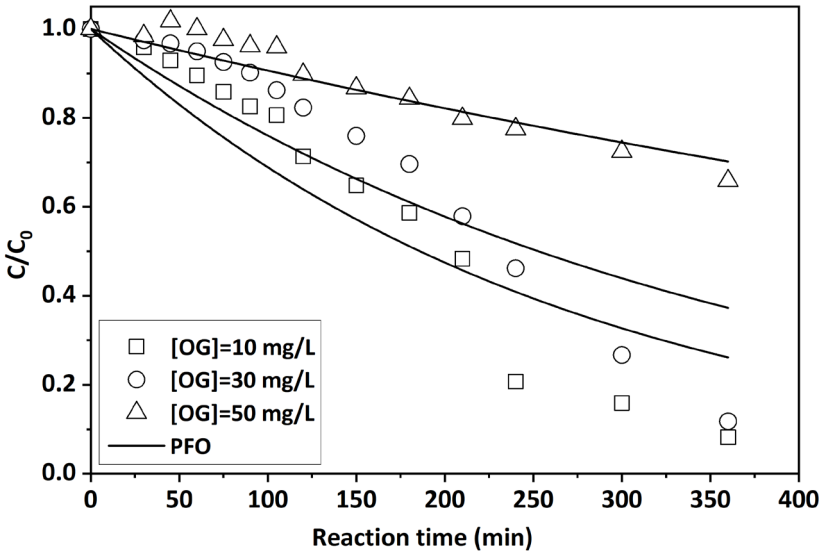

Fig. 8. Photocatalytic degradation kinetics of OG with Ti-SBA-15 (2 g/L). Normalized concentration (C/C_0) versus time and corresponding pseudo-first-order PFO (-), at varying initial OG concentrations (10 (□), 30 (○), and 50 (Δ) mg/L).

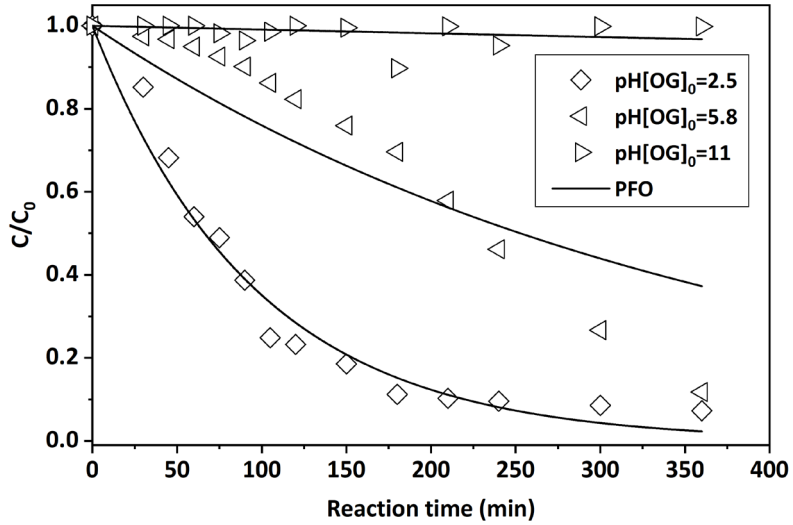

Fig. 9. Effect of initial solution pH on the photocatalytic degradation of OG over Ti-SBA-15. Normalized concentration (C/C_0) versus time and corresponding pseudo-first-order kinetic fits (-) at different pH values (pH=2.5 (□), pH= 5.8 (○), pH=11 (Δ)).

The most notable finding was the significant pH-dependent variation in k (see Fig. 9). The rate was maximized under strongly acidic conditions (k = 1.046 × 10^{-2} min^{-1} at pH = 2.5), reduced under near-neutral pH conditions (k = 2.74 × 10^{-3} min^{-1} at pH = 5.8) and almost completely suppressed under basic pH values

(k = 9.18 × 10^{-5} min^{-1} at pH = 11.0). This behaviour can be explained by electrostatic interactions governed by the Point of Zero Charge (PZC ~ 4.1) of Ti-SBA-15 [26]. Below the PZC, the attraction between the protonated surface and the negatively charged OG leads to a build-up. Above the PZC, repulsion creates a barrier. This slows down the process. These results emphasize the importance of interfacial electrostatics as a rate-limiting factor [9, 10, 12, 30].

3.5.3. Quantification of the Stability Function

One of the main objectives of this study was to quantify the long-term functional durability of the model system. This was done by conducting photocatalytic cycles consecutively under optimal conditions (2.0 g L^{-1}, pH = 2.5). The overall degradation efficiency was measured at 85.2% in the first cycle, decreasing marginally to 83.5%, 81.0% and 78.8% over the subsequent three cycles (see Fig. 10). Normalizing these results to the initial cycle shows that 92.5% of the relative activity was retained after the fourth cycle. There was an average loss of less than 2.1% per cycle.

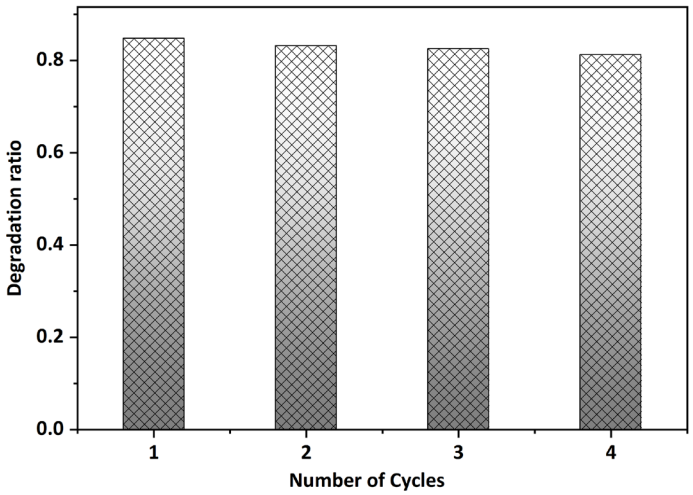

Fig. 10. Photocatalytic reusability of Ti-SBA-15 over four consecutive cycles.

This minimal decay is a sign of its stability. The central hypothesis is also supported by the findings. The primary deactivation pathways of leaching and aggregation are effectively suppressed by the structural confinement of isolated Ti^{4+} sites within the rigid silica framework. These are typical of nanoparticle composites [10, 31]. This outcome is in line with the anticipated reliability of framework-integrated locations, as reported in [13, 14]. It corroborates the hypothesis that engineered architecture engenders a stable functional interface.

4. Conclusions

In this investigation, we employed a logical design approach to effectively generate a clearly defined photocatalytic model system comprising a mesoporous SBA-15 silica framework with atomically dispersed, isolated Ti^{4+} sites. We synthesized this framework using a direct, one-pot method. A thorough examination confirmed the formation of this architecture. The most important proof was the growth of the lattice and the presence of a special LMCT band at 220 nm , and the lack of crystalline TiO_2 phases.

This system can be used to effectively explore the relationship between nanoscale confinement, electronic structure and functional durability. Kinetic analysis of the photo-oxidative degradation of OG yielded an apparent rate constant of $k = 0.01046$ min^{-1} under optimal conditions. By systematically varying catalyst loading, probe concentration and solution pH, the process mechanisms have been found.

The central finding of this study is that exceptional operational stability is an intrinsic property of the material. The confined Ti^{4+} sites exhibited minimal activity decay (less than 2.1% per cycle) and retained over 92.5% efficiency across four consecutive uses. This robustness validates our core hypothesis: the spatial and electronic confinement of active centres within an inert matrix can suppress common deactivation pathways.

This study demonstrates that engineered atomic dispersion within a porous host degrades dyes and creates stable, functional interfaces where durability is inherent to the architecture. Thus, robust materials can be designed, with applications in heterogeneous catalysis, sensing and energy conversion.

R E F E R E N C E S

[1] *N.W. Ashcroft, N.D. Mermin*, Solid State Physics, Cengage Learning, 1976.
[2] *B.H. Bransden, C.J. Joachain*, Physics of Atoms and Molecules, Pearson Education, 2003.
[3] *A.L. Linsebigler, G. Lu, J.T. Yates*, Photocatalysis on TiO_2 surfaces: principles, mechanisms, and selected results, Chem. Rev., Vol. **95**, Iss. 3, 1995. DOI: 10.1021/cr00035a013.
[4] *D.W. Bahnemann*, Photocatalytic water treatment: solar energy applications, Solar Energy, Vol. **77**, Iss. 5, 2004. DOI: 10.1016/j.solener.2004.03.031.
[5] *T. Peng, D. Zhao, K. Dai, W. Shi, K. Hirao*, Synthesis of titanium dioxide nanoparticles with mesoporous anatase wall and high photocatalytic activity, J. Phys. Chem. B, Vol. **109**, Iss. 11, 2005. DOI: 10.1021/jp044771r.
[6] *Y. Shiraishi, N. Saito, T. Hirai,* Adsorption-driven photocatalytic activity of mesoporous titanium dioxide, J. Am. Chem. Soc., Vol. **127**, Iss. 37, 2005. DOI: 10.1021/ja053265s.
[7] *L. Mahoney, R.T. Koodali*, Versatility of evaporation-induced self-assembly (EISA) method for preparation of mesoporous TiO_2 for energy and environmental applications, Materials, Vol. **7**, Iss. 4, 2014. DOI: 10.3390/ma7042697.
[8] *E. Parra-Ortiz, L. Caselli, M. Agnoletti, M.W.A. Skoda, X. Li, D. Zhao, M. Malmsten*, Mesoporous silica as a matrix for photocatalytic titanium dioxide nanoparticles: lipid membrane interactions, Nanoscale, Vol. **14**, Iss. 33, 2022. DOI: 10.1039/d2nr01958b.

[9] *W.Y. Jung, S.H. Baek, J.S. Yang, K.T. Lim, M.S. Lee, G.D. Lee*, et al., Synthesis of Ti-containing SBA-15 materials and studies on their photocatalytic decomposition of orange II, Catal. Today, Vol. **131**, Iss. 1-4, 2008. DOI: 10.1016/j.cattod.2007.10.072.

[10] *H. Lachheb, O. Ahmed, A. Houas, J.P. Nogier*, Photocatalytic activity of TiO_2–SBA-15 under UV and visible light, J. Photochem. Photobiol. A: Chem., Vol. **226**, Iss. 1, 2011. DOI: 10.1016/j.jphotochem.2011.09.017.

[11] *O. Levenspiel*, Chemical Reaction Engineering, John Wiley & Sons, 1999.

[12] *A.J. Bard, L.R. Faulkner*, Electrochemical Methods: Fundamentals and Applications, John Wiley & Sons, 2000.

[13] *W.H. Zhang, J. Lu, B. Han, M. Li, J. Xiu, P. Ying, C. Li*, Direct synthesis and characterization of titanium-substituted mesoporous molecular sieve SBA-15, Chem. Mater., Vol. **14**, Iss. 8, 2002. DOI: 10.1021/cm011686c.

[14] *P. Wu, T. Tatsumi, T. Komatsu, T. Yashima*, Postsynthesis, characterization, and catalytic properties in alkene epoxidation of hydrothermally stable mesoporous Ti-SBA-15, Chem. Mater., Vol. **14**, Iss. 4, 2002. DOI: 10.1021/cm010910v.

[15] *S.K. Das, M.K. Bhunia, A. Bhaumik*, Highly ordered Ti-SBA-15: efficient H_2 adsorbent and photocatalyst for eco-toxic dye degradation, J. Solid State Chem., Vol. **183**, Iss. 6, 2010. DOI: 10.1016/j.jssc.2010.04.015.

[16] *Y. Awoke, Y. Chebude, C. Márquez-Álvarez, I. Díaz*, Solvent free epoxidation of vernonia oil using Ti-SBA-15 with tailor made particle morphology and pore size, Catal. Today, Vol. **345**, 2020. DOI: 10.1016/j.cattod.2019.09.024.

[17] *P.H.K. Charan, G.R. Rao*, Textural and morphological studies of transition metal doped SBA-15 by co-condensation method, J. Chem. Sci., Vol. **127**, Iss. 5, 2015. DOI: 10.1007/s12039-015-0847-5.

[18] *L. Ruchomski, J. Ozimek, K. Siedliska, K.N. Raftopoulos, K. Pielichowski*, Characterization of Ti/SBA-15 composites synthesized by chemical vapour deposition of organic titanium compounds, Crystals, Vol. **13**, Iss. 2, 2023. DOI: 10.3390/cryst13020288.

[19] *N.O. Ramoraswi, P.G. Ndungu*, Photo-catalytic properties of TiO_2 supported on MWCNTs, SBA-15 and silica-coated MWCNTs nanocomposites, Nanoscale Res. Lett., Vol. 10, 2015. DOI: 10.1186/s11671-015-1137-3.

[20] *X.N. Pham, M.B. Nguyen, H.V. Doan*, Direct synthesis of highly ordered Ti-containing Al-SBA-15 mesostructured catalysts from natural halloysite and its photocatalytic activity for oxidative desulfurization of dibenzothiophene, Adv. Powder Technol., Vol. **31**, Iss. 8, 2020. DOI: 10.1016/j.apt.2020.06.028.

[21] *Y. Huang, Y. Jia, R. Hou, Z. Huang, K. Shen, G. Jin, L. Hou,* Photocatalytic degradation of unsymmetrical dimethylhydrazine on TiO_2/SBA-15 under 185/254 nm vacuum-ultraviolet, RSC Adv., Vol. **11**, Iss. 39, 2021. DOI: 10.1039/d1ra03599a.

[22] *V.P. Barba, B. Selvaratnam, P. Thangarasu, R.T. Koodali*, How porous periodicity of mesoporous materials like TiO_2-SBA-15-10 encourages photocatalytic degradation of rhodamine B: a comparative study with aperiodic TiO_2-SiO_2-aerogel-10, J. Porous Mater., Vol. 28, 2021. DOI: 10.1007/s10934-021-01151-8.

[23] *S.C. Göl, E. Akbay*, Reusable TiO_2-SBA-15 synthesized by different silica/titania ratios for photodegradation, ChemistrySelect, Vol. **8**, Iss. 36, 2023. DOI: 10.1002/slct.202301887.

[24] *H.T.T. Duong, M.T.P. Duong, O.K. Nguyen, S.T. Le, L.V. Dang,* et al., Photocatalytic activity of Ti-SBA-15/C_3N_4 for degradation of 2,4-dichlorophenoxyacetic acid in water under visible light, J. Anal. Methods Chem., Vol. **2022**, 2022. DOI: 10.1155/2022/5531219.

[25] *E. Sacaliuc, A.M. Beale, B.M. Weckhuysen, T.A. Nijhuis,* Propene epoxidation over Au/Ti-SBA-15 catalysts, J. Catal., Vol. **248**, Iss. 2, 2007. DOI: 10.1016/j.jcat.2007.03.014.

[26] *G. Almohammadi, C. O'Modhrain, S. Kelly, J.A. Sullivan*, Ti-doped SBA-15 catalysts used in phenol oxidation reactions, ACS Omega, Vol. **5**, Iss. 1, 2020. DOI: 10.1021/acsomega.9b03530.

[27] *M. Kujbida, A. Wróblewska, G. Lewandowski, M. Bosacka, Z.C. Koren, B. Michalkiewicz*, Effect of surface hydrophobization on the 1,5,9-cyclododecatriene epoxidation process with hydrogen peroxide on silanized Ti-SBA-15 catalyst, J. Ind. Eng. Chem., Vol. **121**, 2023. DOI: 10.1016/j.jiec.2023.02.002.

[28] *W.Y. Jung, K.T. Lim, S.S. Park, G.D. Lee, S.S. Hong*, Synthesis of TiO_2 supported on SBA-15 using chelating method and their photocatalytic decomposition of methylene blue, J. Nanosci. Nanotechnol., Vol. **11**, Iss. 1, 2011. DOI: 10.1166/jnn.2011.3207.

[29] *M.B. Gholivand, M.M. Abolghasemi, P. Fattahpour*, Polypyrrole/hexagonally ordered silica nanocomposite as a novel fiber coating for solid-phase microextraction, Anal. Chim. Acta, Vol. **704**, Iss. 1-2, 2011. DOI: 10.1016/j.aca.2011.07.045.

[30] *M.J. López-Muñoz, R. van Grieken, J. Aguado, J. Marugán*, Role of the support on the activity of silica-supported TiO_2 photocatalysts: structure of the TiO_2/SBA-15 photocatalysts, Catal. Today, Vol. **101**, Iss. 3-4, 2005. DOI: 10.1016/j.cattod.2005.03.017.

[31] *J.Q. Wei, X.J. Chen, P.F. Wang, Y.B. Han, J.C. Xu, B. Hong*, et al., High surface area TiO_2/SBA-15 nanocomposites: synthesis, microstructure and adsorption-enhanced photocatalysis, Chem. Phys., Vol. **510**, 2018. DOI: 10.1016/j.chemphys.2018.05.012.